Journal of Magnetic Resonance **138,** 173–177 (1999)
Article ID jmre.1999.1713, available online at http://www.idealibrary.com on IDEAL®

Asymmetric Adiabatic Pulses for NH Selection

Tsang-Lin Hwang,* Peter C. M. van Zijl,* and Michael Garwood†

**Department of Radiology and Biophysics and Biophysical Chemistry, Johns Hopkins University School of Medicine, 217 Traylor Building, 720 Rutland Avenue, Baltimore, Maryland 21205; and †Center for Magnetic Resonance Research and Department of Radiology, 2021 6th Street Southeast, University of Minnesota, Minneapolis, Minnesota 55455*

Received September 1, 1998; revised December 29, 1998

Many types of NMR experiments demand the use of frequency-selective pulses to invert magnetization within discrete frequency limits. For certain experiments, only one side of the inversion band must be sharply demarcated, in which case this transition bandwidth can be narrowed when using an asymmetric adiabatic full passage. In the present study, a highly efficient asymmetric adiabatic full passage was created from a combination of two adiabatic half passages which used different modulation functions (HS_2^1 and tanh/tan). Each adiabatic half passage occupied a different amount of time in the total pulse and performed one-half of the inversion. On one side, HS_2^1 produced a sharp transition between inverted and noninverted states which was approximately 2.5 times narrower than the transition bandwidth afforded by a symmetric hyperbolic secant pulse of equal length. On the other side of the narrow transition band, the tanh/tan pulse achieved broadband inversion. These asymmetric pulses were applied to select NH groups immediately adjacent to the water signal in water-flipback HSQC experiments using a double spin echo for the reverse INEPT step.

Key Words: **adiabatic full passage; asymmetric pulses; selective spin inversion.**

In certain NMR experiments, it is desirable to excite peaks selectively on one side of a spectral region, while leaving other peaks untouched. For example, a pulse that has a sharp transition between noninverted and inverted states can be used in HSQC (*1*) experiments to refocus NH groups while avoiding interference from water signals. Recently, Rosenfeld *et al.* (*2–4*) derived asymmetric pulses that are based on the principles of adiabatic full passage (AFP). These pulses produce an asymmetric distribution of magnetization across the inversion bandwidth, with the transition band on one side being much narrower than that on the other side. Such pulses were originally designed for use in fat-suppressed MRI, in which the lipid methyl and methylene protons are selectively inverted and suppressed using WEFT (*5*). Of the different asymmetric AFPs described (*2–4*), the smallest transition bandwidth was attained with a pulse generated via a modified version of the optimization procedure known as NOM (numerically optimized modulation) (*6, 7*). With a 20-ms pulse length and $\gamma B_1^{\max}/2\pi = 1$ kHz, this pulse (*4*) generated an inversion bandwidth of close to 1150 Hz, with a transition bandwidth of only 77 Hz, which is about 40% of the transition bandwidth produced by a hyperbolic secant pulse (HS1) (*8, 9*) of equal length. Here we demonstrate how asymmetric AFPs can be created from a combination of two different adiabatic half passages that employ modulation functions having analytical form. Simulations and experiments show that these new pulses offer improved performance as judged by their ability to achieve a narrow transition band immediately adjacent to a broadband inversion. These pulses are applied to select NH signals in Fast-HSQC (FHSQC) (*10*) experiments.

In a frequency-modulated (FM) frame of reference which rotates with the instantaneous frequency of the pulse $\omega(t)$, the transverse and longitudinal field components (in frequency units) are

$$\boldsymbol{\omega_1}(t) = \omega_1^{\max} F_1(t)\hat{\mathbf{x}}' \quad [1]$$

$$\begin{aligned}\boldsymbol{\Delta\omega}(t) &= [\omega_o - \omega(t)]\hat{\mathbf{z}}' \\ &= [\boldsymbol{\Omega} - AF_2(t)]\hat{\mathbf{z}}',\end{aligned} \quad [2]$$

where $\omega_1^{\max}$ $(=\gamma B_1^{\max})$ and A are the amplitudes of the modulation functions, $F_1(t)$ and $F_2(t)$ are dimensionless shape functions with values in the range of 0 to 1 and -1 to 1, respectively, ω_0 is the Larmor frequency, and $\boldsymbol{\Omega}$ is the resonance offset when $AF_2(t) = 0$. In the FM frame, the effective field $\boldsymbol{\omega}_{\text{eff}}$ that a magnetization vector experiences is simply the vector sum of the components given by Eqs. [1] and [2].

Tannús and Garwood (*11*) and Kupče and Freeman (*12*) have developed an analytical procedure to derive modulation functions that ensure a constant adiabaticity for all isochromats $\boldsymbol{\Omega}$ inside the sweep range when $\boldsymbol{\omega}_{\text{eff}}$ is crossing the transverse plane (i.e., when $\Delta\omega(t) = 0$ and $\omega_{\text{eff}}(t) = \gamma B_1^{\max}$). When an AFP has this property, the pulse is said to possess offset-independent adiabaticity (OIA) (*11*). To derive OIA pulses, the FM function ($AF_2(t)$) can be calculated by integrating the square of the AM function $\omega_1(t)$, which can be any continuous function which best satisfies the requirements at hand. For example, with the OIA pulse known as HS*n* (*11*), the time variable in the sech function is raised to its *n*th power for the

1090-7807/99 $30.00

purpose of reducing the peak B_1 amplitude. The AM and FM functions can be written as

$$\mathrm{AM}(\tau) = \omega_1^{\max} \mathrm{sech}(\beta\tau^n) \quad [3]$$

$$\mathrm{FM}(\tau) = A \int_0^{\tau} \mathrm{sech}^2(\beta\tau'^n) d\tau', \quad [4]$$

where τ is normalized time ($=2t/T_p$, while T_p is the pulse length) defined in the interval $-1 \leq \tau \leq 1$, and β is a truncation factor, which for our purposes, is chosen such that $\mathrm{sech}(\beta) = 0.01$.

With an AFP, the transition bandwidths are determined by the specific AM function used, provided that the frequency sweep range ($\pm A$) is larger than the intrinsic bandwidth produced by this AM function by itself (*11*). For example, as n increases in HSn and the AM function approaches a rectangular shape, the transition regions in the inversion profile become less sharp. Conversely, by setting $n < 1$, the width of the transition regions decreases at a cost of increased B_1 amplitude. Likewise, the transition bandwidth can be narrowed using other similar AM shapes that approach a delta function, such as the Lorentzian function (*11, 12*).

By numerically solving the Bloch equation, we determined the widths of the transition regions afforded by HS1, HSn ($n < 1$), and the Lorentzian pulse. For convenience, the different inversion pulses were described by the dimensionless variable R defined as (*13, 14*)

$$R = A \cdot T_p/\pi = bw \cdot T_p, \quad [5]$$

where bw is the total bandwidth of the frequency sweep (in Hertz) and T_p is the pulse length in seconds. The nomenclature used here to describe each AFP is [AM/FM functions, R value used to construct the pulse]. The transition bandwidths were compared among [HS1, $R = 5.56$], [HS_2^1, $R = 5.56$], [HS_3^1, $R = 5.56$], and [Lorentzian, $R = 5.56$]. Unless specified otherwise, all comparisons were performed with $T_p = 2$ ms and $\gamma B_1^{\max}/2\pi = 15$ kHz, and the transition bandwidth was defined as the frequency range in which $-0.95 < M_z/M_0 < 0.95$. The transition bandwidths of [HS_2^1, $R = 5.56$] and of [Lorentzian, $R = 5.56$] were roughly the same, and were two-thirds of the transition bandwidth of [HS1, $R = 5.56$]. To reach acceptable performance, [HS_3^1, $R = 5.56$] required a much higher peak B_1 amplitude with only marginal reduction in the transition bandwidth. Therefore, we used HS_2^1 pulses in the work described below.

Recently, we have demonstrated the ability to perform fast broadband inversion using AM and FM functions based on hyperbolic tangent (tanh) and tangent (tan), respectively (*15*). For example, when using [tanh/tan, $R = 110$] with $T_p = 192$ μs and $\gamma B_1^{\max}/2\pi = 20$ kHz, inversion efficiency corresponding to $M_z/M_0 < -0.98$ can be achieved across a bandwidth of about 40 kHz. This AFP can be constructed from the following adiabatic half passage and its time-reversed adiabatic half passage (*7, 16*), with AM and FM functions given by

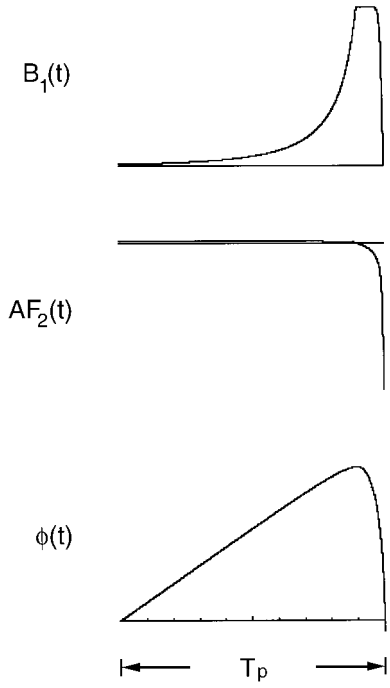

FIG. 1. Asymmetric adiabatic inversion pulse of length T_p composed of the first half of the AFP [HS_2^1, $R = 10$] for 0.9 T_p and the second half of the AFP [tanh/tan, $R = 100$] for 0.1 T_p. $B_1(t)$, $\mathrm{AF}_2(t)$, and $\phi(t)$ represent the shapes of the AM, FM, and phase-modulated (PM) functions, respectively. With most spectrometers, implementation can be simplified by using the PM function instead of the FM function.

$$\mathrm{AM}(t) = \omega_1^{\max} \tanh[\xi 2t/T_p] \quad [6]$$

$$\mathrm{FM}(t) = A \frac{\tan[\kappa(1 - 2t/T_p)]}{\tan[\kappa]}, \quad [7]$$

where $\xi = 10$, $\tan[\kappa] = 20$, and $0 \leq t \leq T_p/2$.

Considering that HS_2^1 is capable of producing a sharp transition, while the tanh/tan pulse can achieve fast broadband inversion, a combination of these two types of pulses was expected to yield an efficient asymmetric AFP. We first used 7200 points to sample the shape of [HS_2^1, $R = 10$] and 800 points for [tanh/tan, $R = 100$], and then combined the first half of [HS_2^1, $R = 10$] and the second half of [tanh/tan, $R = 100$] to form the asymmetric adiabatic pulse shown in Fig. 1, denoted [HS_2^1, $R = 10$, 0.9 T_p; tanh/tan, $R = 100$, 0.1 T_p]. HS_2^1 and tanh/tan accounted for 0.9 and 0.1 T_p, respectively.

For [HS1, $R = 5.56$], [HS_2^1, $R = 5.56$], and [HS_2^1, $R = 10$, 0.9 T_p; tanh/tan, $R = 100$, 0.1 T_p], the relative transition bandwidths were 1, $\frac{2}{3}$, and $\frac{1}{2}$, respectively (Fig. 2). The different R values were necessary to center the transition regions at the same offset, but do not affect the transition widths. These

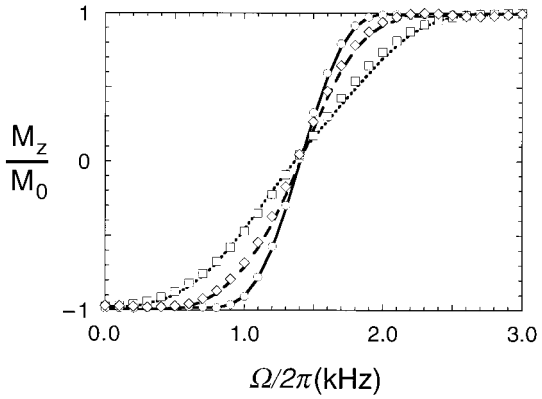

FIG. 2. Simulated transition band for different inversion pulses: [HS1, $R = 5.56$] (···), [HS^1_2, $R = 5.56$] (– – –), and [HS^1_2, $R = 10$, 0.9 T_p; tanh/tan, $R = 100$, 0.1 T_p] (—), and their correspondingly experimental profiles: [HS1, $R = 5.56$] (□), [HS^1_2, $R = 5.56$] (◇), and [HS^1_2, $R = 10$, 0.9 T_p; tanh/tan, $R = 100$, 0.1 T_p] (○). All of the pulses were set to $T_p = 2$ ms, and $\gamma B_1^{max}/2\pi = 15.0$ kHz during the simulations and experiments.

pulses were tested on a Varian UnityPlus 500-MHz spectrometer equipped with a 5-mm triple-resonance PFG probe, RF waveform generator, and a shielded z gradient unit. Inversion experiments, {180°—G—90°—acquire}, were performed on a sample of 1% H_2O in D_2O, doped with 0.1 mg/ml $GdCl_3$. Figure 2 also shows that the experimental inversion performance agrees with Bloch equation simulations.

Figure 3 shows a contour plot of the simulated M_z/M_0 profiles that are produced with [HS^1_2, $R = 10$, 0.9 T_p; tanh/tan, $R = 100$, 0.1 T_p] when using $T_p = 2$ ms. As γB_1^{max} increases, the width of the transition region gradually increases (a phenomenon that also occurs with other pulses (*4*), including HS1). In the inverted region, the bandwidth increases as γB_1^{max} increases, due to the use of tan frequency sweep (*9*, *15*, *17*). It should be noted that both γB_1^{max} and the $\boldsymbol{\Omega}$ axis scale inversely

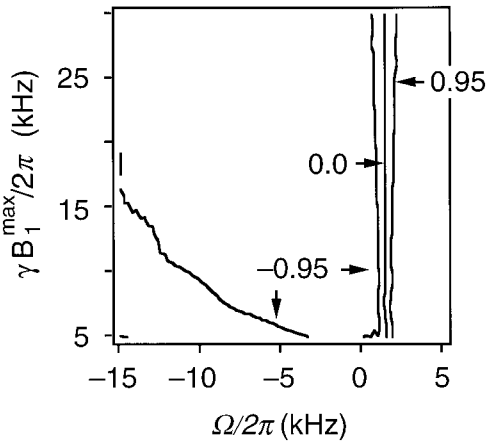

FIG. 3. Simulated inversion contours of [HS^1_2, $R = 10$, 0.9 T_p; tanh/tan, $R = 100$, 0.1 T_p] as a function of resonance offset $\boldsymbol{\Omega}$ and RF amplitude γB_1^{max}. $T_p = 2$ ms. Contour levels are labeled in terms of M_z/M_0.

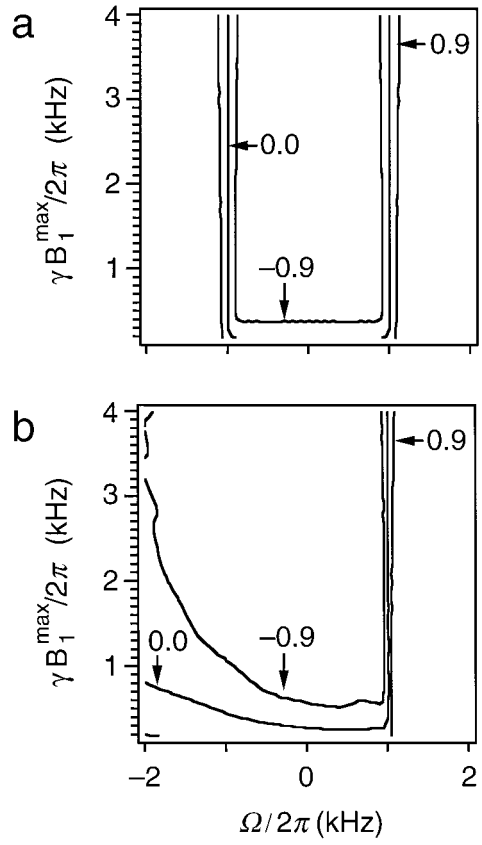

FIG. 4. Simulated inversion contours of (a) [HS1, $R = 40$] and (b) [HS^1_2, $R = 76$, 0.95 T_p; tanh/tan, $R = 70$, 0.05 T_p] as a function of resonance offset $\boldsymbol{\Omega}$ and RF amplitude γB_1^{max}. $T_p = 20$ ms. Contour levels are labeled in terms of M_z/M_0.

with T_p. Other pulse parameters (e.g., β, ξ, and κ) can also be adjusted to tune the performance of asymmetric adiabatic pulses.

Rosenfeld *et al.* (*4*) compared the performance of [HS1, $R = 40$] with their numerically optimized asymmetric AFP using $T_p = 20$ ms. A similar asymmetric adiabatic pulse can also be created using HS^1_2 and tanh/tan; namely, [HS^1_2, $R = 76$, 0.95 T_p; tanh/tan, $R = 70$, 0.05 T_p]. In this pulse, HS^1_2 with $R = 76$ was used to center the sharp transition band at $\boldsymbol{\Omega}/2\pi = 1$ kHz. Figure 4 shows the M_z/M_0 contours of [HS1, $R = 40$] and [HS^1_2, $R = 76$, 0.95 T_p; tanh/tan, $R = 70$, 0.05 T_p] as a function of $\boldsymbol{\Omega}$ and γB_1^{max} for $T_p = 20$ ms. [HS^1_2, $R = 76$, 0.95 T_p; tanh/tan, $R = 70$, 0.05 T_p] achieves a narrow transition and wide inversion bandwidths. Table 1 lists the transition and inversion bandwidths produced by the different pulses described above.

Figure 5 compares the peak intensities from the first increment of 2D FHSQC (*10*) experiments with different NH detection schemes in the reverse INEPT (*18*) step. The experiments were performed on a Varian Unity Inova 800-MHz spectrometer equipped with a 5-mm triple-resonance PFG probe, RF waveform generator, and a shielded triple-axis gra-

TABLE 1
Calculated Transition and Inversion Bandwidths at Various γB_1^{max} and T_p for Different Adiabatic Pulses

Pulse	T_p(ms)[a]	$\gamma B_1^{max}/2\pi$ (kHz)	Transition bandwidth (kHz)[b]	Inversion bandwidth (kHz)[c]
[HS^1_2, R = 10, 0.9 T_p; tanh/tan, R = 100, 0.1 T_p]	2	15	0.916	15.2
	2	10	0.788	11.7
	20	1	0.079	1.2
[HS^1_2, R = 76, 0.95 T_p; tanh/tan, R = 70, 0.05 T_p]	20	1	0.077	1.7
[HS1, R = 40]	20	1	0.197	1.8

[a] T_p = 2 ms for water suppression in FHSQC, while T_p = 20 ms for lipid suppression in WEFT.
[b] Defined as the frequency range in which $-0.95 < M_z/M_0 < 0.95$.
[c] Defined as the frequency range in which $-1 < M_z/M_0 < -0.95$.

dient unit. The sample was 1.5 mM ^{15}N-labeled staphylococcal nuclease at pH 6.8 and 25°C. For comparison purposes, the WATERGATE 3—9—19 module (*19*) was first applied to obtain the spectrum for the NH region (Fig. 5a). Figure 5b was obtained with a double-echo approach (*20*) using [HS^1_2, R = 10, 0.9 T_p; tanh/tan, R = 100, 0.1 T_p] for ^{1}H and [HS1, R = 60, 0.9 T_p; tanh/tan, R = 70, 0.1 T_p] for ^{15}N. Figure 5c was obtained in an identical manner, except [HS1, R = 33.4] and [HS1, R = 20] were used for the ^{1}H and ^{15}N pulses, respectively. A phase ramp for an offset of 2000 and 9900 Hz was added to [HS^1_2, R = 10, 0.9 T_p; tanh/tan, R = 100, 0.1 T_p] and [HS1, R = 33.4], respectively, to avoid exciting the water resonance. When T_p = 2 ms, the transition bandwidths for [HS1, R = 33.4] and [HS1, R = 5.56] are similar, and the inversion bandwidths are 14.6 and 0.7 kHz, respectively. Unlike WATERGATE, the adiabatic double-echo sequence provided optimal performance for a wide range of RF power settings, and can be applied to the adiabatic version of FHSQC experiments for automation purposes (*21*). Since the evolution due to coupling constants J is reduced during adiabatic pulses (*22–24*), the period used in the reverse INEPT step had to be extended to 6.2 ms when using the AFPs (Figs. 5b and 5c), while it was 5.6 ms with WATERGATE (Fig. 5a). With the asymmetric pulse (Fig. 5b), the peak intensities were roughly the same as those obtained with WATERGATE (Fig. 5a). The spectrum obtained with the symmetric pulse (Fig. 5c) shows significantly reduced peak intensities toward the water resonance, in accordance with the simulation which predicted the transition bandwidth to be ~2.1 kHz (Fig. 2).

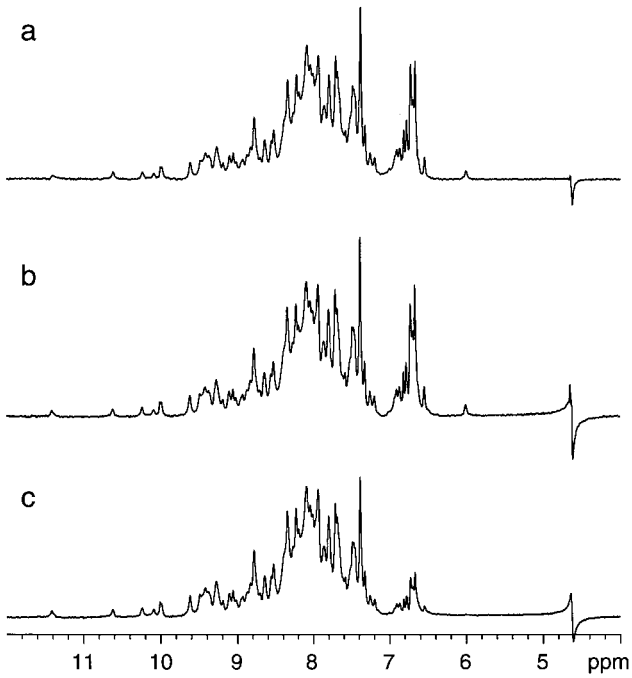

FIG. 5. Spectra obtained from the first increment of FHSQC experiments with different NH detection schemes. (a) The WATERGATE 3—9—19 module with interpulse delay = 150 μs. (b) [HS^1_2, R = 10, 0.9 T_p; tan h/tan, R = 100, 0.1 T_p] for ^{1}H and [HS1, R = 60, 0.9 T_p; tanh/tan, R = 70, 0.1 T_p] for ^{15}N. (c) [HS1, R = 33.4] for ^{1}H and [HS1, R = 20] for ^{15}N. In (b) and (c), the proton AFPs were applied using $\gamma B_1^{max}/2\pi$ = 14.7 kHz and T_p = 2 ms. All other ^{1}H pulses were applied at $\gamma B_1^{max}/2\pi$ = 37.9 kHz and the ^{15}N pulses at 7.2 kHz. GARP decoupling (*25*) was used at 1.5 kHz.

In conclusion, we have shown that asymmetric inversion pulses constructed from tanh/tan and HS^1_2 functions can yield broadband inversion while creating a sharp transition on one side of the inversion profile. These pulses have been exploited in water-flip-back HSQC experiments to select NH groups while avoiding excitation of water. Pulse parameters (e.g., R, T_p) can be easily adjusted to optimally meet other experimental needs.

ACKNOWLEDGMENTS

The authors thank Dr. David Shortle for providing the staphylococcal nuclease sample. The 800-MHz spectrometer at the University of Minnesota was supported by NSF Grant BIR-9601477. This research was supported by NIH Grants RR11115 (P.v.Z.) and RR08079 (M.G.), and, in part, via a subcontract of NIH STTR Grant GM55441 to Adiabatics, Inc., of which M.G. and P.v.Z. are officers. The terms of this agreement have been reviewed and approved by the Johns Hopkins University in accordance with its conflict of interest policies.

REFERENCES

1. G. Bodenhausen and D. J. Ruben, Natural abundance nitrogen-15 NMR by enhanced heteronuclear spectroscopy, *Chem. Phys. Lett.* **69,** 185–189 (1980).
2. D. Rosenfeld, S. L. Panfil, and Y. Zur, Analytic solutions of the Bloch equation involving asymmetric amplitude and frequency modulations, *Phys. Rev. A* **54,** 2439–2443 (1996).
3. D. Rosenfeld, S. L. Panfil, and Y. Zur, Design of adiabatic pulses for fat-suppression using analytic solutions of the Bloch equation, *Magn. Reson. Med.* **37,** 793–801 (1997).
4. D. Rosenfeld, S. L. Panfil, and Y. Zur, Design of selective adiabatic inversion pulses using the adiabatic condition, *J. Magn. Reson.* **129,** 115–124 (1997).
5. S. L. Patt and B. D. Sykes, Water eliminated Fourier transform NMR spectroscopy, *J. Chem. Phys.* **56,** 3182–3184 (1972).
6. K. Uğurbil, M. Garwood, and A. R. Rath, Optimization of modulation functions to improve insensitivity of adiabatic pulses to variations in B_1 magnitude, *J. Magn. Reson.* **80,** 448–469 (1988).
7. M. Garwood and K. Uğurbil, B_1 insensitive adiabatic RF pulses, in "NMR, Basic Principles and Progress" (M. Rudin, Ed.), Vol. 26, pp. 109–147, Springer-Verlag, Berlin (1992).
8. M. S. Silver, R. I. Joseph, and D. I. Hoult, Highly selective $\pi/2$ and π pulse generation, *J. Magn. Reson.* **59,** 347–351 (1984).
9. J. Baum, R. Tycko, and A. Pines, Broadband and adiabatic inversion of a two-level system by phase-modulated pulses, *Phys. Rev. A* **32,** 3435–3447 (1985).
10. S. Mori, C. Abeygunawardana, M. O'Neil Johnson, and P. C. M. van Zijl, Improved sensitivity of HSQC spectra of exchanging protons at short interscan delays using a new fast HSQC (FHSQC) detection scheme that avoids water saturation, *J. Magn. Reson. B* **108,** 94–98 (1995).
11. A. Tannús and M. Garwood, Improved performance of frequency-swept pulses using offset-independent adiabaticity, *J. Magn. Reson. A* **120,** 133–137 (1996).
12. Ē. Kupče and R. Freeman, Optimized adiabatic pulses for wideband spin inversion, *J. Magn. Reson. A.* **118,** 299–303 (1996).
13. Y. Ke, D. G. Schupp, and M. Garwood, Adiabatic DANTE sequences for B_1-insensitive narrowband inversion, *J. Magn. Reson.* **96,** 663–669 (1992).
14. T.-L. Hwang, M. Garwood, A. Tannús, and P. C. M. van Zijl, Reduction of sideband intensities in adiabatic decoupling using modulation generated through adiabatic *R*-variation (MGAR), *J. Magn. Reson. A* **121,** 221–226 (1996).
15. T.-L. Hwang, P. C. M. van Zijl, and M. Garwood, Fast broadband inversion by adiabatic pulses, *J. Magn. Reson.* **133,** 200–204 (1998).
16. M. Garwood and Y. Ke, Symmetric pulses to induce arbitrary flip angles with compensation for RF inhomogeneity and resonance offsets, *J. Magn. Reson.* **94,** 511–525 (1991).
17. C. J. Hardy, W. A. Edelstein, and D. Vatis, Efficient adiabatic fast passage for NMR population inversion in the presence of radiofrequency field inhomogeneity and frequency offsets, *J. Magn. Reson.* **66,** 470–482 (1986).
18. G. A. Morris and R. Freeman, Enhancement of nuclear magnetic resonance signals by polarization transfer, *J. Am. Chem. Soc.* **101,** 760–762 (1979).
19. V. Sklenár, M. Piotto, R. Leppik, and V. Saudek, Gradient-tailored water suppression for ^{1}H–^{15}N HSQC experiments optimized to retain full sensitivity, *J. Magn. Reson. A* **102,** 241–245 (1993).
20. T.-L. Hwang and A. J. Shaka, Water suppression that works. Excitation sculpting using arbitrary waveforms and pulsed field gradients, *J. Magn. Reson. A* **112,** 275–279 (1995).
21. P. C. M. van Zijl, T.-L. Hwang, M. O'Neil Johnson, and M. Garwood, Optimized excitation and automation for high-resolution NMR using B_1 insensitive rotation pulses, *J. Am. Chem. Soc.* **118,** 5510–5511 (1996).
22. M. R. Bendall, Heteronuclear J coupling procession during spin-lock and adiabatic pulses. Use of adiabatic inversion pulses in high-resolution NMR, *J. Magn. Reson. A* **116,** 46–58 (1995).
23. Ē. Kupče and R. Freeman, Compensation for spin-spin coupling effects during adiabatic pulses, *J. Magn. Reson.* **127,** 36–48 (1997).
24. C. Zwahlen, S. J. F. Vincent, and L. E. Kay, Analytical description of the effect of adiabatic pulses on IS, I_2S, and I_3S spin systems, *J. Magn. Reson.* **130,** 169–175 (1998).
25. A. J. Shaka, P. B. Barker, and R. Freeman, Computer-optimized decoupling scheme for wideband applications and low-level operation, *J. Magn. Reson.* **64,** 547–552 (1985).